AIP | The Journal of Chemical Physics

Rotational constants and structure of para-difluorobenzene determined by femtosecond Raman coherence spectroscopy: A new transient type

Takuya Den, Hans-Martin Frey, Peter M. Felker, and Samuel Leutwyler

Citation: The Journal of Chemical Physics **143**, 144306 (2015); doi: 10.1063/1.4932602
View online: http://dx.doi.org/10.1063/1.4932602
View Table of Contents: http://scitation.aip.org/content/aip/journal/jcp/143/14?ver=pdfcov
Published by the AIP Publishing

THE JOURNAL OF CHEMICAL PHYSICS **143**, 144306 (2015)

Rotational constants and structure of *para*-difluorobenzene determined by femtosecond Raman coherence spectroscopy: A new transient type

Takuya Den,[1] Hans-Martin Frey,[1] Peter M. Felker,[2] and Samuel Leutwyler[1,a)]
[1]*Departement für Chemie und Biochemie, Universität Bern, Freiestrasse 3, CH-3000 Bern 9, Switzerland*
[2]*Department of Chemistry and Biochemistry, University of California at Los Angeles, 607 Charles E. Young Drive East, Los Angeles, California 90095-1569, USA*

(Received 17 July 2015; accepted 25 September 2015; published online 12 October 2015)

Femtosecond Raman rotational coherence spectroscopy (RCS) detected by degenerate four-wave mixing is a background-free method that allows to determine accurate gas-phase rotational constants of non-polar molecules. Raman RCS has so far mostly been applied to the regular coherence patterns of symmetric-top molecules, while its application to nonpolar asymmetric tops has been hampered by the large number of RCS transient types, the resulting variability of the RCS patterns, and the 10^3–10^4 times larger computational effort to simulate and fit rotational Raman RCS transients. We present the rotational Raman RCS spectra of the nonpolar asymmetric top 1,4-difluorobenzene (*para*-difluorobenzene, *p*-DFB) measured in a pulsed Ar supersonic jet and in a gas cell over delay times up to ~2.5 ns. *p*-DFB exhibits rotational Raman transitions with $\Delta J = 0, 1, 2$ and $\Delta K = 0, 2$, leading to the observation of $J-$, $K-$, $A-$, and C–type transients, as well as a novel transient (S–type) that has not been characterized so far. The jet and gas cell RCS measurements were fully analyzed and yield the ground-state ($v = 0$) rotational constants A_0 = 5637.68(20) MHz, B_0 = 1428.23(37) MHz, and C_0 = 1138.90(48) MHz (1σ uncertainties). Combining the A_0, B_0, and C_0 constants with coupled-cluster with single-, double- and perturbatively corrected triple-excitation calculations using large basis sets allows to determine the semi-experimental equilibrium bond lengths r_e(C$_1$–C$_2$) = 1.3849(4) Å, r_e(C$_2$–C$_3$) = 1.3917(4) Å, r_e(C–F) = 1.3422(3) Å, and r_e(C$_2$–H$_2$) = 1.0791(5) Å. © *2015 AIP Publishing LLC.* [http://dx.doi.org/10.1063/1.4932602]

I. INTRODUCTION

Fluorinated compounds are rare in nature but are widely used in pharmaceuticals, medicine, and for agricultural applications. A major trend in pharmaceutical chemistry has been to introduce F atoms to change the chemical and physicochemical properties (such as the hydro/lipophilicity, H-bonding properties, and biodegradability) of previously known pharmaceutically active molecules.

In order to treat the effects of H/F substitution by quantum chemistry, highly correlated methods with very large basis sets must be used, since the high nuclear charge of the F atom increases the relative importance of electron correlation. Thus, the performance of both the computational methods and the basis sets must be benchmarked for fluorinated compounds; for this, accurate experimental data are needed. Demaison *et al.* have examined the experimentally available high-accuracy experimental structures and bond lengths of fluorobenzenes with one to six fluorine atoms, and compared these to the predictions of coupled-cluster with single-, double- and perturbatively corrected triple-excitations [CCSD(T)] calculations using systematically larger basis sets.[1] The accurate structural data from microwave spectroscopy were only available for non-centrosymmetric (and hence polar) fluorobenzenes,[1] while inversion-symmetric molecules are not accessible by microwave spectroscopy. Using femtosecond (fs) Raman rotational coherence spectroscopy (RCS), the Bern group has previously determined rotational and centrifugal distortion constants for the symmetric tops 1,3,5-trifluorobenzene (TFB) and hexafluorobenzene (HFB) by fitting the experimental RCS transients.[2,3] Combining these results with CCSD(T) correlated calculations allowed to determine semiexperimental C–F and C–C bond lengths.[1–3]

Para-difluorobenzene (*p*-DFB), shown in Figure 1, is also nonpolar. However, compared to the treatments of the symmetric top molecules TFB and HFB, the asymmetric-top Raman RCS simulations are significantly more involved: First, the asymmetric-top rotational eigenfunctions and energy eigenvalues $E(J, K_1, K_{-1})$ must be computed numerically, in contrast to symmetric tops whose rotational level energies can be expressed analytically. Second, the rotational Raman transition intensities of symmetric tops are given analytically by the Placzek-Teller factors,[4,5] which involve only a few multiplication and division operations, while for asymmetric tops, the evaluation of the rotational Raman intensities involves $\sim J^3$ floating-point operations.[4] Third, the three different diagonal (in some cases also off-diagonal) components of the molecular polarizability tensor of asymmetric-top molecules give rise to different rotational transient types.[6–8] Thus, the computational time required to generate asymmetric-top Raman RCS transients is typically 10^3–10^4 times larger than for symmetric-rotor RCS transients.

The C–C and C–F bond lengths of gas-phase *p*-DFB have previously been determined by Domenicano *et al.* using the

a)leutwyler@iac.unibe.ch

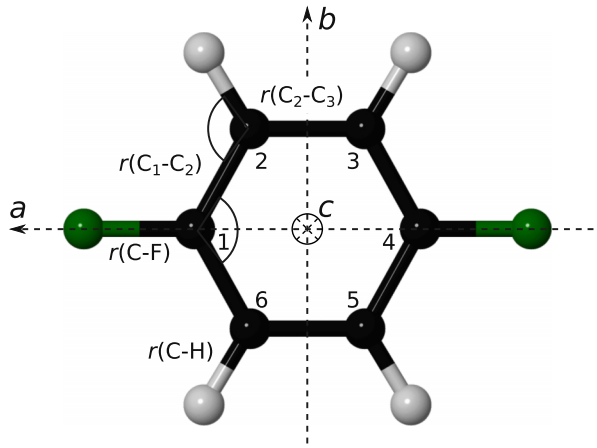

FIG. 1. CCSD(T)/cc-pwCVTZ calculated equilibrium structure of *para*-difluorobenzene, C-atom numbering, structure parameter definition and molecular inertial axes $\{a, b, c\}$.

gas-phase electron diffraction (GED) method, which yields r_g bond lengths that are thermally averaged at the experimental temperature (~300 K).[9] They obtained r_g(C–C)$_{mean}$ =1.392(3) Å, r_g(C–H)=1.088(5) Å, and r_g(C–F)=1.354(4) Å. The C_5–C_1–C_2 ring angle at the *ipso*–F carbon was determined to be 123.5(1)°. To date, the accurate ground-state rotational constants of *p*-DFB are only known from theoretical studies or model structures.[1,10] The rotational constants of *p*-DFB were estimated in 1970 by Hollas *et al.*,[10] based on a substitution model of benzene and a set of substituted benzenes. For *p*-DFB, they estimate rotational constants A = 5639.1, B = 1428.2, and C = 1139.5 MHz, based on which they determined S_1 state rotational constants of *p*-DFB by rotational band contour analysis of the 0_0^0 band.[11] In a study by Neusser *et al.*, the rotational constants of the 27_0^1 vibronic band were also obtained by rotational band contour analysis.[12] More recently, Riehn *et al.* investigated *p*-DFB and the *p*-DFB· Ar van der Waals complex using RCS spectroscopic methods.[13–15] For *p*-DFB, these workers were not able to fully simulate the transient at that time and did not determine any rotational constants.[15] They determined ground- and excited-state rotational constants for the *p*-DFB· Ar van der Waals complex from time-resolved fluorescence depletion using a near-symmetric oblate-top model.[13–15] Since the Ar atom lies on the *c*-axis of *p*-DFB, the reported A constant (1135.3(6) MHz) can be compared to the C rotational constant of *p*-DFB in this work, see Figure S1[16] of the supplementary material.

In this work, we study the gas-phase rotational motion of *p*-DFB using time-resolved femtosecond Raman RCS, detected by degenerate four-wave mixing (DFWM) both in a supersonic jet and in a room-temperature gas cell. We are able to simulate the asymmetric-top Raman RCS transients in detail, allowing us to quantitatively fit the experimental RCS transient and determine the ground-state rotational constants A_0, B_0, and C_0. We find evidence for a new type of rotational transient, denoted S-type. By combining the experimental rotational constants with coupled-cluster CCSD(T) calculations using large basis sets, we have determined the semiexperimental[1,17–20] independent structure parameters of *p*-DFB, i.e., the C_1–C_2, C_2–C_3, C–F, and C–H bond lengths and two bond angles.

A. Methods

1. Experimental methods

The fs degenerate four-wave mixing setup at the University of Bern has been previously described.[2,20,21] Briefly, three parallel laser beams from an amplified Ti:Sapphire laser system provide the ~75 fs pulses at 800 nm employed for the stimulated Raman pump, dump, and probe steps. The stimulated Raman polarization induced by the pump/dump steps at time zero is detected by the DFWM signal generated from the time-delayed probe pulse. The energy of the three laser pulses is ~100 μJ/pulse per beam. The three pulse trains are spatially overlapped and focused by an f = 1000 mm achromatic lens in a folded BOXCARS[22] arrangement. For the supersonic jet experiments, in which intermolecular collisions that lead to decoherence of the rotational wave packet are strongly reduced, the *p*-difluorobenzene (Sigma Aldrich, ≥99% purity) is heated to 70 °C, mixed with Ar carrier gas to a total backing pressure of p_0 = 400 mbar and sent through a pulsed valve (0.45 mm nozzle diameter) operating at a repetition rate of 333 Hz. The supersonic jet expands into a ~0.1 mbar vacuum. The DFWM mixing signal is generated in the overlap volume of the three laser beams within the core of the supersonic-jet expansion at a distance of ~2 mm from the nozzle. After the output window of the vacuum chamber, the intense pump, dump, and probe laser pulses are blocked by a mask, while the DFWM signal beam is recollimated, spatially filtered, and detected by a cooled GaAs photomultiplier. The transients are obtained by scanning the delay time in steps of ~20 fs, giving 7 data points on the instrument response function of 140 fs. Analogous measurements were performed in a static gas cell at room temperature (T = 293 K) and a *p*-DFB pressure of 15 mbar.

2. Computational methods

The structure optimizations of *para*-difluorobenzene were first performed using the second-order Møller Plesset (MP2) method with the cc-pVTZ basis set. Subsequently, the structures were re-optimized using the coupled-cluster CCSD(T) method and the correlation-consistent weighted core-valence polarized cc-pwCVDZ and cc-pwCVTZ basis sets. All electrons were correlated and D_{2h} symmetry was enforced throughout. At the CCSD(T)/pwCVDZ equilibrium geometry, the anharmonic vibrational frequencies and the vibration-dependent rotational constants A_v, B_v, and C_v were calculated with an anharmonic cubic force fields derived using analytical second-derivative techniques.[23] All calculations were carried out with the CFOUR program.[24]

II. ROTATIONAL RAMAN COHERENCE SPECTROSCOPY OF ASYMMETRIC-TOP MOLECULES

A. Modeling the degenerate four-wave mixing signal:

Rotational Raman RCS spectroscopy is a time-dependent variant of DFWM that can be applied to polar and nonpolar molecules.[6–8,13,14,17–20,25–35] In off-resonant four-wave mixing — which is appropriate here, since *p*-DFB is com-

pletely transparent at the 800 nm laser wavelength — the DFWM signal of the gas sample is proportional to the square modulus of its time-dependent third-order susceptibility,[36–38] $\chi^{(3)}(t)$, which can be written as

$$I(t) = \int_{-\infty}^{\infty} G(\tau)|\chi^{(3)}(t-\tau)|^2 d\tau, \tag{1}$$

where $G(t)$ is the experimental apparatus function, which is determined by the triple temporal convolution of the fs Raman pump/dump and probe pulses. $G(t)$ was measured prior to each RCS experiment using the electronic zero-time Kerr-effect signal of the Ar carrier gas in the supersonic jet and is closely represented by a Gaussian of 140–150 fs full width at half maximum. The $\chi^{(3)}(t)$ associated with fs DFWM induced coherences between asymmetric-top rotational states is given by

$$\chi^{(3)}(t) \sim C + \sum_{\Gamma<\Gamma'} b_{\Gamma,\Gamma'} \sin[(E_{\Gamma'} - E_{\Gamma})t/\hbar], \tag{2}$$

where $\Gamma \equiv J_\tau$ and $\Gamma' \equiv J'_{\tau'}$ denote asymmetric-top energy levels, E_Γ and $E_{\Gamma'}$ are their respective energies, $b_{\Gamma,\Gamma'}$ are the modulation amplitudes, and the summation is over all those pairs of levels for which $E_\Gamma < E_{\Gamma'}$. In general, we work at experimental conditions where the background parameter C is zero, as in Figs. 3(a)-3(g), and so C is not a fit parameter.

The dynamic range of the current measurements corresponds to a signal/noise ratio S/N ~ 1000:1 for the strongest recurrences. The weakest recurrences that are used in the RCS fit have S/N ~ 8:1. The main factors determining the signal intensity $I(t)$ (and limiting the significant digits of the derived rotational constants) have been discussed in Ref. 20; very briefly these are (1) the anisotropy of the molecular polarizability tensor $\Delta\alpha$, which is given in the last line of Table III. The signal is proportional to the fourth power of $\Delta\alpha$. (2) The gas-phase density of *p*-DFB at 70 °C, which is the maximum operating temperature of our 333 Hz pulsed valve. For the cell measurement, the current limit is the vapor pressure of the substance at room temperature. The signal $I(t)$ depends on the square of the gas-phase density.

In order to model the degenerate four-wave mixing signal, one first has to calculate the rotational energy levels of an asymmetric top E_Γ and the corresponding rotational eigenfunctions. From these, the rotational Raman transition intensities need to be calculated for all pairs of levels that contribute to the rotational beating. These procedures are detailed in Subsections II B and II C.

B. Energy levels of asymmetric-top molecules

The asymmetric-top energy levels are determined by diagonalization of the asymmetric-top Hamiltonian in a symmetric-top basis, as described in detail in, e.g., Gordy and Cook.[39] By the spectral theorem, the asymmetric-top eigenfunctions $|\Gamma M\rangle$ can be expressed as a linear combination of symmetric-top eigenfunctions $|JKM\rangle$,

$$|\Gamma M\rangle = |J\tau M\rangle = \sum_{K=-J}^{J} a(\Gamma, K)|JKM\rangle, \tag{3}$$

where $\tau = K_{-1} - K_{+1}$ is the difference of the corresponding prolate and oblate symmetric-top state K quantum numbers.

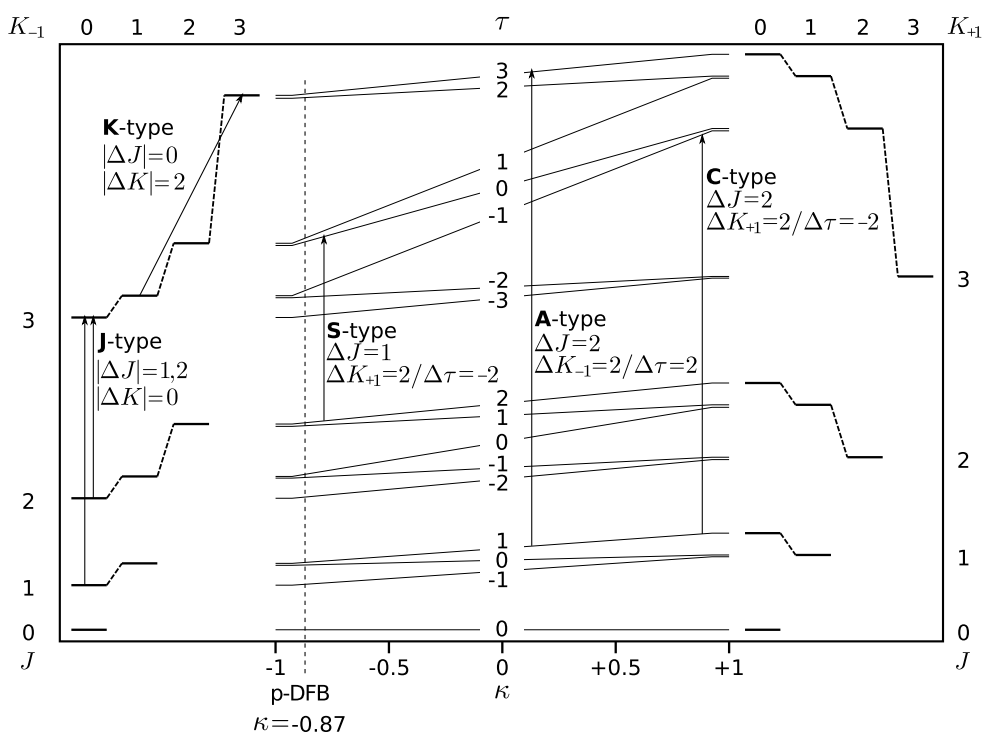

FIG. 2. Center: Schematic rotational energy level scheme for an asymmetric top molecule, as a function of $\kappa = -1.0$ to $+1.0$, corresponding to prolate (left) and oblate (right) symmetric-top limits, see the text. The $\kappa = -0.87$ for *para*-difluorobenzene is marked as a vertical dashed line. Symmetric-top levels with the same $|K|$ values are degenerate, as indicated at the extreme left and right; this degeneracy is lifted in asymmetric tops. The rotational quantum numbers are J, K_{+1}, K_{-1}, $\tau = K_{-1} - K_{+1}$, see the text. Examples of allowed rotational transitions are drawn as arrows, together with the RCS transient types (K-type, J-type, etc.) to which they contribute.

TABLE I. The relationship of the irreducible spherical polarizability components $\alpha_k^{(j)}$ to their molecular polarizability Cartesian counterparts $\alpha_{\rho\sigma}$.[41]

ΔJ	ΔK	$\alpha_k^{(j)}$	$\alpha_{\rho\sigma}$
	2	$\alpha_2^{(2)}$	$\frac{1}{2}[(\alpha_{xx}-\alpha_{yy})+i(\alpha_{xy}+\alpha_{yx})]$
±2	1	$\alpha_1^{(2)}$	$-\frac{1}{2}[(\alpha_{xz}+\alpha_{zx})+i(\alpha_{yz}+\alpha_{zy})]$
±1	0	$\alpha_0^{(2)}$	$\frac{1}{\sqrt{6}}(2\alpha_{zz}-(\alpha_{xx}+\alpha_{yy}))$
0	−1	$\alpha_{-1}^{(2)}$	$\frac{1}{2}[(\alpha_{xz}+\alpha_{zx})-i(\alpha_{zy}+\alpha_{yz})]$
	−2	$\alpha_{-2}^{(2)}$	$\frac{1}{2}[(\alpha_{xx}-\alpha_{yy})-i(\alpha_{xy}+\alpha_{yx})]$

The subscripts −1 and +1 refer to Ray's asymmetry parameter $\kappa = (2B_0 - A_0 - C_0)/(A_0 - C_0)$, where the prolate symmetric-top limit corresponds to $\kappa = -1$ and the oblate symmetric-top limit to $\kappa = +1$. As usual, $K = J, J-1, \ldots, -J$ denotes the projection of the total angular momentum J on the major molecule-fixed principal axis, which for p-DFB is the a-axis, as indicated in Figure 1.

The rotational energy levels of an asymmetric-top molecule lie between the prolate and oblate limits, as shown in Figure 2. In contrast to symmetric-top states, which are degenerate for J-states with the same absolute K value, no such degeneracy exists in asymmetric tops. In fact, K is not a good quantum number for asymmetric-tops, instead states are specified by J and τ.[39,40] However, for molecules that are only slightly asymmetric, K_1 and K_{-1} are still approximately good quantum numbers. The rotational Raman selection rules that are discussed below are those for a prolate asymmetric top with $K \sim K_{-1}$.

TABLE II. Characteristic asymmetric-top rotational coherence transient types.

Transient type	Position t[a]	Contributing rotational transitions
	Symmetric top transients	
J-type[b]	$n/2(B+C)$	$\lvert\Delta J\rvert = 1, 2$ $\lvert\Delta K\rvert = 0$
K-type[b]	$n/(4A-2B-2C)$	$\lvert\Delta J\rvert = 0$ $\lvert\Delta K\rvert = 2$
	Asymmetry transients[c]	
A-type[b]	$n/4A$	$\Delta J = 2$ $\Delta K_1 = 0$ $\Delta K_{-1} = 2$
C-type[b]	$n/4C$	$\Delta J = 2$ $\Delta K_1 = 2$ $\Delta K_{-1} = 0$
S-type	$n/(B+C)$	$\Delta J = 1$ $\Delta K_1 = 2$ $\Delta K_{-1} = 0$

[a]Position is estimated based on a prolate symmetric-top.
[b]From Refs. 7 and 8.
[c]Transients involving $\lvert\Delta K\rvert = 1$ do not occur for p-DFB, since the off-diagonal components of the polarizability tensor are zero, see Table I.

C. Rotational Raman selection rules and Raman intensities for asymmetric tops

The rotational Raman selection rules pertaining to the pairs of levels $|\Gamma M\rangle$ and $|\Gamma' M'\rangle$ that contribute to Eq. (2) are established by finding non-zero values of the rotational Raman transition moment $\langle\Gamma' M'|\widehat{\alpha}|\Gamma M\rangle$, where $\widehat{\alpha}$ is the 3×3 molecular polarizability tensor, defined in a molecule-fixed Cartesian axis system. For a detailed derivation for symmetric tops, see Ref. 41. With our choice of the molecule-fixed coordinate system for p-DFB, $\alpha_{zz} = \alpha_{aa}$, $\alpha_{yy} = \alpha_{bb}$, and $\alpha_{xx} = \alpha_{cc}$.

The analogous procedure can be applied to asymmetric-top states, as these can be written as a superposition of symmetric-top states, see Eq. (3). An elegant way to deal with the

TABLE III. Calculated equilibrium and vibrationally averaged rotational constants, A-reduced centrifugal distortion constants and molecular polarizability tensor of p-difluorobenzene.

Rotational constants/MHz	MP2/ cc-pVDZ	MP2/ cc-pVTZ	CCSD(T)/ cc-pwCVDZ	CCSD(T)/ cc-pwCVTZ
A_e	5606.3773	5729.6911	5583.1890	5682.0176
B_e	1404.4182	1436.6530	1401.2265	1429.6374
C_e	1123.0820	1148.6440	1120.1098	1142.2412
A_0	5559.1102	5683.4993	5533.7189	
B_0	1398.3884	1429.8832	1395.1471	
C_0	1117.2885	1142.4076	1114.1976	
$\Delta_A = A_e - A_0$	47.2671	46.1917	49.4701	
$\Delta_B = B_e - B_0$	6.0298	6.7697	6.0795	
$\Delta_C = C_e - C_0$	5.7935	6.2366	5.9122	
Centrifugal distortion constants/kHz				
Δ_j	0.0352	0.0367	0.0354	
Δ_k	1.0060	1.0513	1.0083	
Δ_{jk}	0.0448	0.0491	0.0475	
δ_j	0.0082	0.0085	0.0082	
δ_k	0.1403	0.1465	0.1412	
Polarizability tensor elements/bohr^3				
α_{aa}	71.7	74.1	72.0	
α_{bb}	71.8	73.1	72.1	
α_{cc}	25.1	33.8	25.3	
$\alpha_{off-diagonal}$	0	0	0	
$(2\alpha_{aa}-\alpha_{bb}-\alpha_{cc})/(\alpha_{bb}-\alpha_{cc})$	0.9957	1.0508	0.9957	

rotational Raman transition moment integrals is to decompose α into irreducible spherical polarizability tensor components, $\alpha_k^{(j)}$, and then use angular momentum coupling rules.[41] The $\alpha_k^{(j)}$ can be regarded as angular momentum states $|J = j, K = k\rangle$, where k runs from $-j$ to $+j$. Detailed analysis shows that for p-DFB, only the tensor components $\alpha_k^{(2)}$ contributes to the RCS signal. Each element in $\alpha_k^{(2)}$ can be constructed as a linear combination of the molecular Cartesian polarizability tensor components in the way shown in Table I. In principle the detailed shape of the RCS transient allows to fit the relative ratio of the different $\alpha_k^{(2)}$ contributions. Also, the dependence of the allowed changes in K quantum number on the molecular polarizability tensor components allows deeper insight into the simulated RCS transient: For example, if one is interested only in coherences with $\Delta J = 1, 2$ and $\Delta K = 0$, the molecular polarizability is set to values such that $\alpha_{xx} = \alpha_{yy} \neq \alpha_{zz}$ and $\alpha_{off-diagonal} = 0$.

D. Rotational Raman transient types

For rotational quantum beats to be produced according to Eq. (2), the rotational transition frequencies must be correlated in a specific way, otherwise the individual sine terms interfere destructively and no time dependence on $\chi^{(3)}$ is observed. Constructive interference is possible if two conditions hold: (1) The individual terms have to be phase locked. This is imposed by the experimental conditions as the coherent rotational wavepacket is explicitly created by the stimulated Raman pump and dump pulses. (2) The transition frequencies $(E(\Gamma') - E(\Gamma))/\hbar$ must be correlated. Regular frequency spacing can be shown to occur for (rigid) symmetric-top rotors, e.g., $E(J, K) = BJ(J + 1) + (A - B)K^2$ for a prolate symmetric top.[8] In asymmetric tops, for which the frequency regularities of symmetric-tops do not apply, one might expect that the time-dependent part of $\chi^{(3)}$ does not survive thermal averaging. However, Felker and co-workers have shown that even for

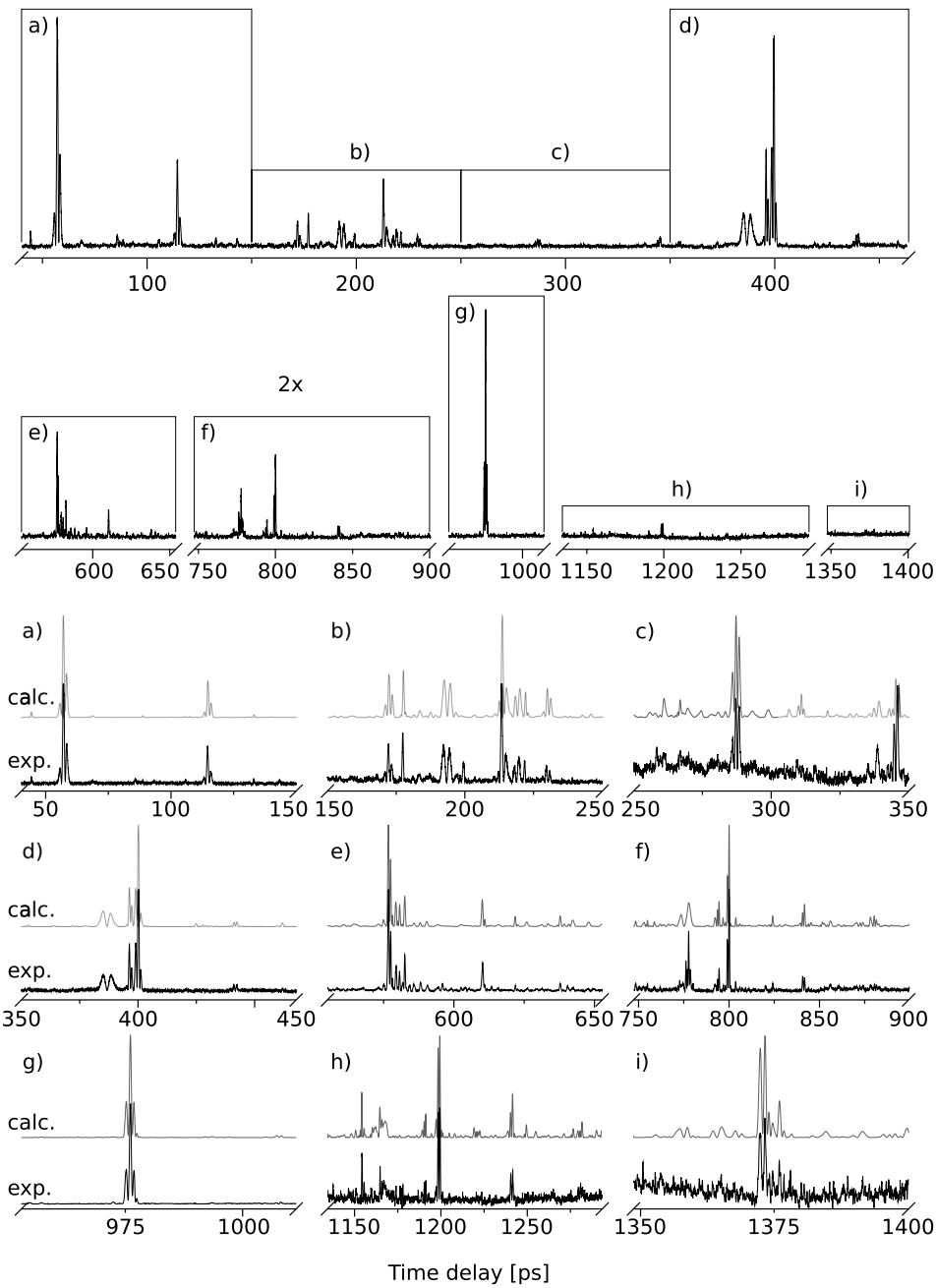

FIG. 3. Experimental and simulated femtosecond rotational Raman RCS spectrum of p-DFB in a supersonic-jet for delay time $t = 50$–1400 ps ($T_{rot} = 130$ K). The two top panels show the complete RCS spectrum; (a)-(i) show magnified subsections of ~100 ps length.

TABLE IV. CCSD(T)/cc-pwCVDZ calculated vibrational frequencies (in cm^{-1}) up to ν_{15}, vibrational populations (in %) at 130 K and 293 K, and the three calculated rotation-vibration constants $\alpha_v^{A,B,C}$ (in MHz).

Normal mode	Wavenumber	Population (130 K)	Population[a] (293 K)	α_v^A	α_v^B	α_v^C
Ground state	0	77.5	25.1	0	0	0
ν_7	159.5	13.3	11.7	26.15	−0.64	−1.06
ν_8	342.4	1.8	4.9	−24.23	0.08	0.47
ν_9	377.4	1.2	4.1	65.06	−0.88	−0.82
ν_{10}	422.1	0.7	3.3	5.06	−0.19	−0.56
ν_{11}	437.3	0.6	3.1	−62.61	−0.19	1.15
ν_{12}	448.5	0.5	2.9	−0.81	−0.11	−0.65
ν_{13}	522.0	0.2	2.1	−0.48	0.17	−0.46
ν_{14}	637.6	0.1	1.2	6.89	−0.02	0.34
ν_{15}	656.6	0.1	1.1	−5.38	−0.22	−0.45

[a]Vibrational partition function truncated at 1000 cm^{-1}.

very asymmetric molecules, significant subsets of the rotational levels retain sufficiently regular frequency spacings.[6,8,42] These subsets produce transients that are characterized by their recurrence time and polarity. Transients are named either by their main contributing coherences (J-type and K-type) or by the rotational constants about which they convey information (A-type and C-type). Relevant transient types are listed in Table II and shown in Figure 2.[8,39] Note that a coherence

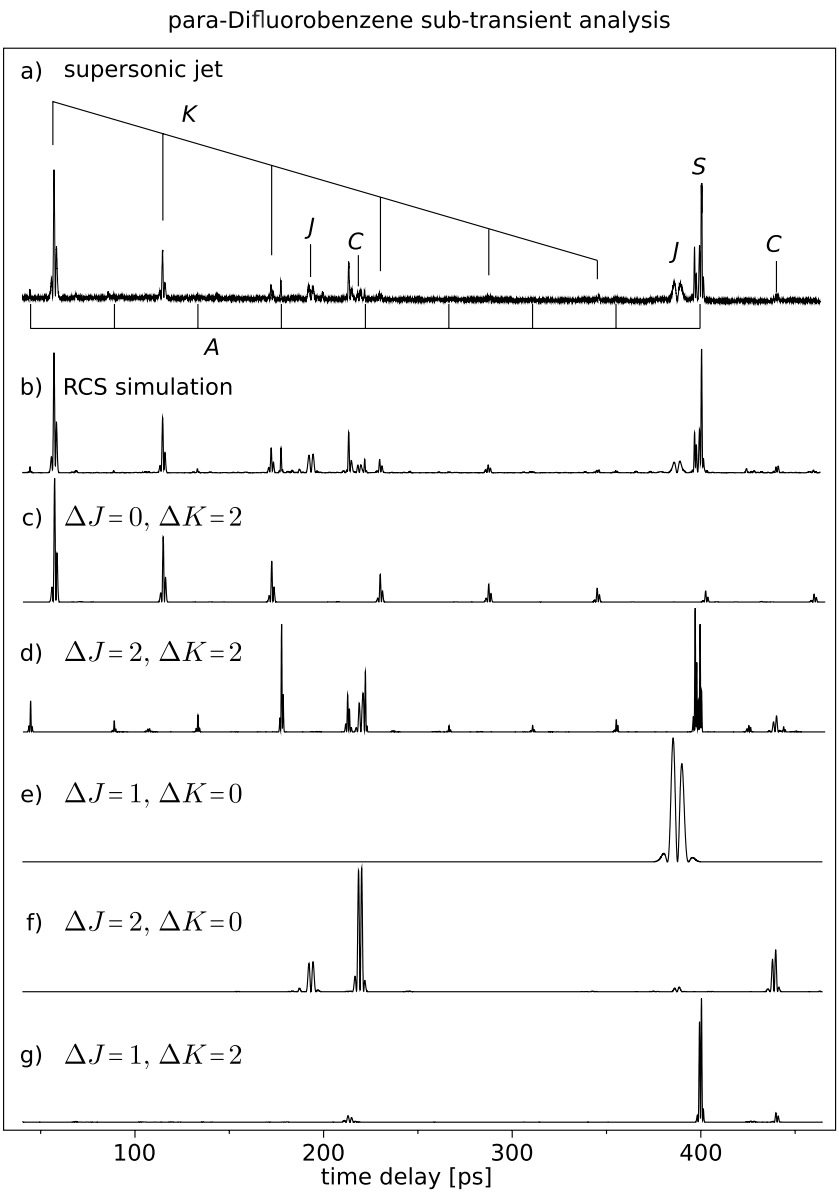

FIG. 4. Detailed assignment of the supersonic-jet rotational RCS transient of p-DFB for time delays t = 40–470 ps: (a) complete experimental transient, (b) complete simulated transient, (c)-(g) simulated sub-transients generated by restricting the coherences to specific ΔJ, ΔK changes.

TABLE V. Ground state rotational constants (in MHz) of p-difluorobenzene determined by different methods.

Constant	CCSD(T)/cc-pwCVTZ[a]	fs-DFWM[b]	S_0/S_1 state model[c]
A_0	5682.02	5637.68(19)	5639.1
B_0	1429.64	1428.23(37)	1428.2
C_0	1142.24	1138.90(48)	1139.5

[a]CCSD(T)/cc-pwCVTZ calculated A_e, B_e and C_e corrected by CCSD(T)/cc-pwCVDZ calculated Δ_A, Δ_B and Δ_C from Table III.
[b]$\pm 1\sigma$ uncertainties in parentheses.
[c]Reference 10.

specified by a specific $\Delta J, \Delta K$ cannot always be assigned to a single transition type. Thus, p-DFB coherences with $\Delta J = 2, \Delta K_{-1} = 0$ contribute intensity to both J-type as well as C-type transients.

E. Fitting procedure and data analysis

The asymmetric-top rotational coherence transients are generated and fitted to the experimental RCS signals using an IDL (Interactive Data Language) program (RSI, Inc.) that employs a Levenberg-Marquardt nonlinear least-squares fit. The program for calculating the asymmetric-top states and the rotational Raman transition amplitudes is written in FORTRAN. The evaluation of the transients is parallelized and distributed over 12 processors with a shared library written in C under the OPENMP protocol.

For the rotational constant fit, the initial values A_0, B_0, and C_0 were taken from the CCSD(T)/cc-pwCVDZ calculations, see Table III. The highest rotational level considered in the simulations was $J_{max} = 150$, corresponding to a cumulative rotational population of ~99% at $T = 130$ K, which is the rotational temperature in the supersonic jet, see below. The measured apparatus function was $G(t) = 140$ fs. The A-reduced centrifugal distortion constants and the α_{aa} and α_{cc} components of the molecular polarizability tensor were taken from the CCSD(T)/cc-pwCVDZ calculation and were fixed to these values throughout the fit. The parameters that were varied to fit the computed RCS transient to experiment were the rotational constants A_0, B_0, and C_0, and the rotational temperature T_{rot}. The ratio of the polarizability tensor component

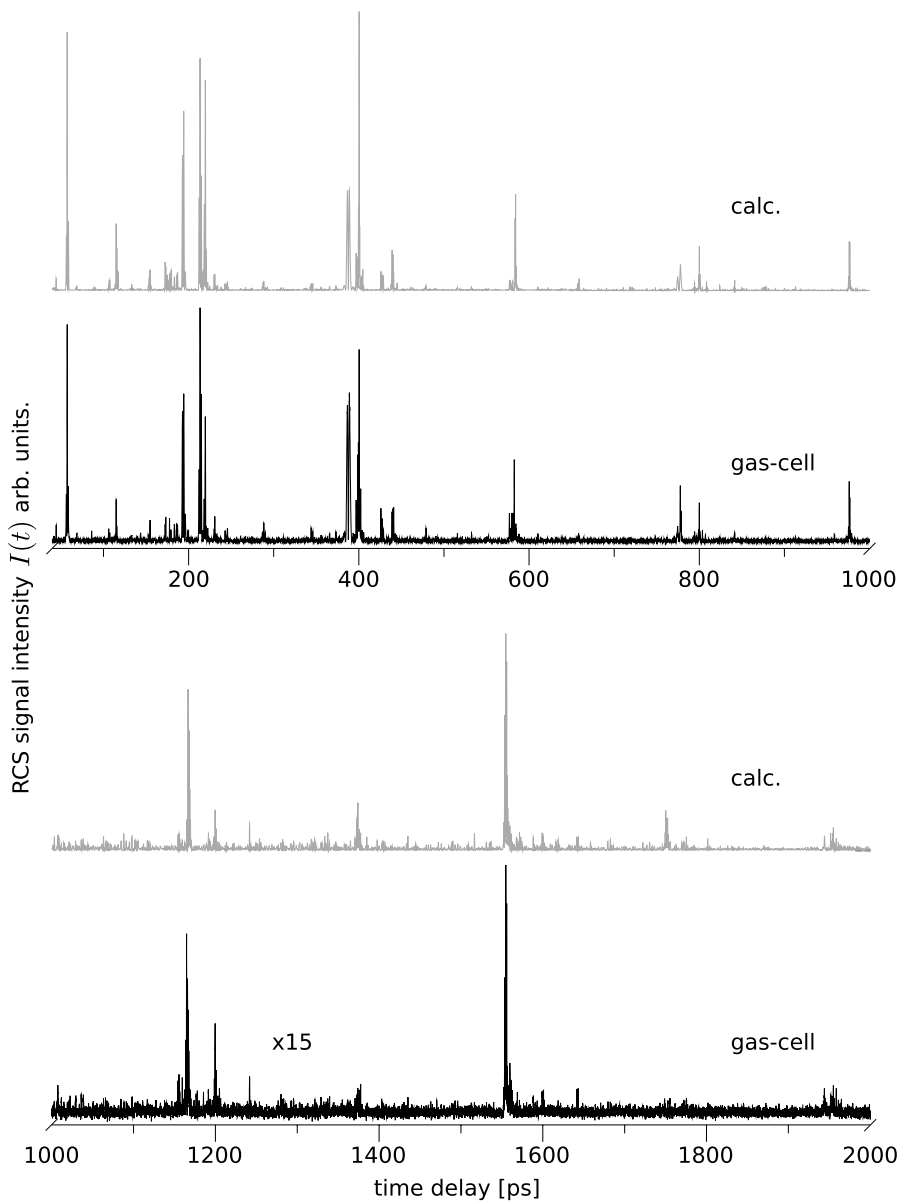

FIG. 5. Top panel: Gas-cell RCS transient ($T = 293$ K) of *para*-difluorobenzene: (a) Comparison of RCS simulation and measurement from $t = 50$–1000 ps, (b) from $t = 1000$–2000 ps. The rich fine structure is well reproduced by the simulation upon including signal contributions from the low-lying vibrational levels ν_7, $2\nu_7$, ν_8, and ν_9, see Figure 6 for details.

α_{bb} relative to α_{aa} and α_{cc} influences the relative intensity of $\Delta K = 0$ and $\Delta K = 2$ transitions, see the last line of Table I. This ratio was fitted in a final fitting round, holding the rotational constants fixed.

III. RESULTS AND DISCUSSION

A. Supersonic jet measurements and assignments

The Raman RCS transient of *p*-DFB in a pulsed Ar supersonic jet was measured over the $t = 0$–1400 ps time range and is shown in Figure 3. From the widths of the recurrences, the effective rotational temperature was determined to be $T_{rot} \sim 130 \pm 5$ K. This value agrees well with the translational temperature $T_{trans} = 130$ K calculated at $x = 2.0$ mm from the nozzle exit. Upstream molecules (closer to the nozzle) are at higher temperature than downstream molecules. The calculated translational temperature change along the jet axis between the upstream and downstream edges of the four-wave mixing overlap area is 3.5 K, i.e., the upstream edge is at 132 K, the downstream edge at 128.5 K. The stated ±5 K uncertainty should be understood to include such spatial averaging effects.

Based on the CCSD(T) harmonic vibrational frequencies given in Table IV (see Table S1 of the supplementary material for a full list),[16] about ~78% of the *p*-DFB population is in the $v = 0$ vibrational ground state at this temperature. Due to the quadratic dependence of $\chi^{(3)}$ on the population of a given level (Eqs. (1) and (2)), the $v = 0$ population accounts for ~97% of the DFWM signal. As mentioned above, we varied α_{bb} to fit the observed ratio of the $\Delta K = 0/\Delta K = 2$ transitions, which is given by $(2\alpha_{aa} - \alpha_{bb} - \alpha_{cc})/(\alpha_{bb} - \alpha_{cc})$. The fitted ratio is 1.04 ± 0.06, which is in good agreement with the CCSD(T) calculated ratios of 0.996–1.051 given in Table III.

There is practically no collisional dephasing in the supersonic jet, as we have shown experimentally for the symmetric-top molecules cyclohexane, trifluorobenzene, and hexafluorobenzene.[2,3,43] Due to the irregular spacing of the transition frequencies in asymmetric-top molecules, their RCS transients decays more rapidly with time than compared to symmetric-top molecules; this is already quite marked given the sizable asymmetry of *p*-DFB with $\kappa = -0.87$. Thus, the RCS transient of hexafluorobenzene shows observable recurrences up to $t \sim 5000$ ps delay,[3] but the last observable recurrences of *p*-DFB lie at $t \sim 1375$ ps, see Figure 3(i).

The asymmetric-top character and the polarizability tensor of *p*-DFB permits transitions with $\Delta J = 0, 1, 2$ and $\Delta K = 0, 2$. We thus expect *J*-, *K*-, *A*-, and *C*-type transients, as shown in Table II. Many features in the RCS transient of *p*-DFB can be straightforwardly assigned based on the expected recurrence times listed in Table II. For a more detailed analysis, we decomposed the RCS transient into sub-transients corresponding to coherences for specific ΔJ and ΔK. This procedure captures interferences between different coherences and allows to assign even small RCS signals to specific transient types. Since asymmetric-top states are eigenfunctions of the total angular momentum J, see Eq. (3), one can restrict ΔJ to select for a subset of transitions. As outlined above, the coherences for specific ΔK transitions are selected by setting specific values for the polarizability tensor elements. Combining ΔJ and ΔK restrictions allows to simulate five different sub-transients, i.e., with $\Delta J = 0/\Delta K = 2$, $\Delta J = 1/\Delta K = 0$, $\Delta J = 2/\Delta K = 0$, $\Delta J = 2/\Delta K = 2$, and $\Delta J = 1/\Delta K = 2$. Note that changes of the K_{-1} or K_1 quantum numbers cannot be selected.

Figure 4 shows the assigned and decomposed transient for $t = 0$–450 ps. The signal at early t is dominated by *K*-type transients spaced by $t = 57$ ps, but these rapidly decay and disappear after for $t = 400$ ps. Small *A*-type transients are observed from 40–200 ps at intervals of $\Delta t = 44$ ps. Two *J*-type transients at multiples of $\Delta t = 193$ ps are also readily identified. *C*-type transients are expected at multiples of $\Delta t = 220$ ps, but there are several signals that qualify as possible candidates around $t = 220$ ps. The assignment is most easily done by comparing to the sub-transient generated by coherences with $\Delta J = 2/\Delta K = 0$, shown in Figure 4(f), which are known to contribute to *C*-type transients. The transient decomposition leads to an unambiguous assignment, but also reveals that the most intense peak at $t = 220$ ps is produced by $\Delta J = 2/\Delta K = 2$ coherences, see Figure 4(d). The latter cannot be assigned to a specific transient type. In fact, many features cannot be assigned to a specific transient type listed in Table II, but one can assign the features to the coherences that produce them.

Interestingly, the strong feature at $t = 400$ ps in Figure 3(d) could not be assigned to any of the transient types defined so far.[7,8] Transient decomposition reveals that this feature is produced mainly by $\Delta J = 1/\Delta K = 2$ coherences, as can be seen in Figure 4(g). In Figure S2[16] of the supplementary material, we show a close-up of this feature and the related recurrences at $t = 800$ ps and $t = 1200$ ps. Coherences with $\Delta J = 2/\Delta K = 2$ also contribute weakly to the signal. However, they are slightly shifted to earlier delay times compared to the coherences with $\Delta J = 1/\Delta K = 2$. To investigate the origin of these transients, we computed the beat amplitude spectrum for *p*-DFB, while restricting the coherences to $\Delta J = \pm 1, \Delta K = \pm 2$. The spectrum shows a significant number of prominent beat peaks spaced by intervals close to 2.5 GHz. These beats seem to originate from $(J,K)/(J+1,K+2)$, $(J+1,K)/(J+2,K+2)$, $(J+2,K)/(J+3,K+2)$, etc., coherences for K values in the vicinity of $J/2$. Such a series of coherences have approximate beat frequencies equal to

$$\begin{aligned}
(J+1)(B+C) + (2A-B-C)(2K+2) &= A(4K+4) + (B+C)(J+1-2K-2),\\
(J+2)(B+C) + (2A-B-C)(2K+2) &= A(4K+4) + (B+C)(J+2-2K-2),\\
\vdots \qquad\qquad &\quad \vdots \qquad\qquad \vdots\\
(J+n)(B+C) + (2A-B-C)(2K+2) &= A(4K+4) + (B+C)(J+n-2K-2).
\end{aligned} \tag{4}$$

When K is in the vicinity of $J/2$, this describes a set of beat peaks spaced by intervals of approximately $(B + C)$ about a central frequency of $A(4K + 4)$. Since $(B + C)$ is close to 2.5 GHz, these beats produce a time-domain feature near t = 400 ps. One can attribute the slight shift of this transient from the J-type recurrence time to asymmetric-rotor effects.

We denote the transients produced by $\Delta J = 1/\Delta K = 2$ coherences S-type, reflecting the "one-ahead and two to the side" movement of a "Springer" (=knight) in chess. There are other small features produced by coherences with $\Delta J = 1/\Delta K = 2$. The small peak at ~440 ps, for example, may contribute intensity C-type transients. The S-type transients are accompanied by small features produced by $\Delta J = 2/\Delta K = 2$ coherences. These features are due to coincidences between A-type transients with $n/2(B + C)$ transients. The large amplitude features in the RCS signal at ~576 ps and 975 ps, see Figures 3(e) and 3(g), are caused by the same coincidences.

B. Determination of rotational constants

The experimental and simulated RCS transients are shown in Figure 3. For the first 450 ps, segments of ~100 ps were fitted in a sliding window fashion with overlaps of ~50 ps. Segments of the transient measured at later delay times were fitted individually. By averaging over 11 individual fit windows, we determined the rotational constants A_0 = 5637.68(19) MHz, B_0 = 1428.23(36) MHz, and C_0 = 1138.90(47) MHz, with the $\pm 1\sigma$ uncertainty given in parentheses. For all fit windows, the rotational temperature remained at around 130 ± 5 K.

The rotational constants of p-DFB determined here and previously are compared in Table V. Our experimental B_0 and C_0 values are very close to B = 1428.2 and C = 1139.5 MHz estimated by Cvitas *et al.* in 1970.[10] However, our experimental A_0 constant is significantly smaller than their estimated value of A = 5639.1 MHz. This is not surprising, as their model

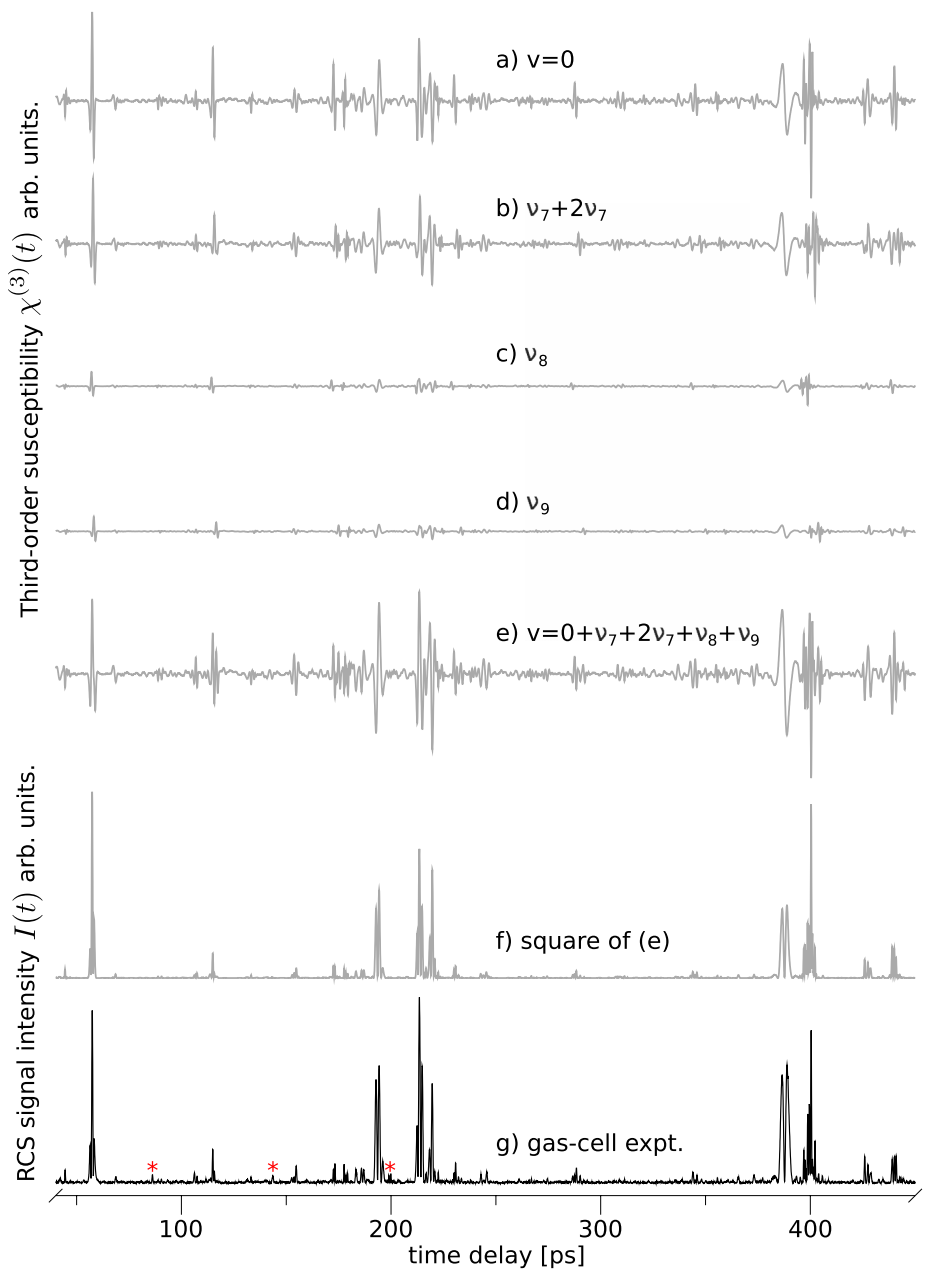

FIG. 6. RCS simulations of the room-temperature gas cell transient measured from t = 40–450 ps time delay. Panels ((a)-(d)) show the contributions of the vibrational states to the third-order susceptibility $\chi^{(3)}(t)$, from (a) $v = 0$ (thermal population 26.2%), (b) $\nu_7 + 2\nu_7$ (total thermal population 17.5%), (c) ν_8 (population 4.9%), and (d) ν_9 (population 4.1%). Panel (e) shows the coherent addition of the ((a)-(d)) vibrational contributions. Panel (f) shows $|\chi^{(3)}|^2(t)$, which is compared to the experimental RCS trace in panel (g). The peaks marked by red asterisks are from a small contamination of the sample, see the text.

did not include changes in C–C or C–H bond lengths upon fluorination.

The rotational constant $A_0 = 1135.3(6)$ MHz of the *p*-DFB· Ar van der Waals complex[13–15] is slightly smaller than the $C_0 = 1138.9(5)$ MHz of *p–DFB* determined here. Since the equilibrium geometry of the Ar atom in *p*-DFB· Ar[13–15,44] is on the *c* inertial axis of *p*-DFB, these rotational constants should be equal for *rigid* *p*-DFB· Ar. The small difference probably arises from the contribution of the vibrational zero-point motion of the Ar atom perpendicular to the *p*-DFB *c* axis. Based on the rotational constants of *p*-DFB· Ar,[13–15] we simulated its Raman RCS transient; no peaks were found that could be assigned to *p*-DFB· Ar.

C. Gas cell measurements

The gas-cell RCS transient of *p*-DFB was measured at $p = 15$ mbar and $T = 293$ K over the time range $t = 0$–2000 ps and is shown in Figure 5. This transient exhibits a rich fine structure that cannot be reproduced by a $v = 0$ simulation at $T = 293$ K, because of the low-lying excited ($v > 0$) vibrational levels that are populated at room temperature, which also contribute to the RCS transient. The v-dependent rotational constants A_v, B_v, and C_v differ significantly from the $v = 0$ rotational constants, as expressed by the rotation-vibration coupling constants α_v^A, α_v^B, and α_v^C.[45] The CCSD(T) calculated values are given in Table IV.

The thermally most strongly populated vibrations are ν_7, ν_8, and ν_9, as shown in Table IV. This Table also shows that the α_v^A values are large, being +26.15, −24.24, and 65.06 MHz, respectively. The α_v^B and α_v^C values are comparatively small, see Table IV. Thus, the contributions from vibrationally excited $v \geq 0$ levels to transient types that depend strongly on A (such as $K-$ and A–type) decrease more rapidly with increasing delay time t than transients that depend on B and C ($J-$, $C-$, and S–type).

The fine structure of the room temperature RCS transient is well reproduced by including the vibrationally excited levels up to ν_9, as shown in Figure 6. Note that the contributions from the levels $v = 0$, ν_7, $2\nu_7$, ν_8, and ν_9 to $\chi^{(3)}$, shown individually in Figures 6(a)-6(d), must be added coherently as in Figure 6(e), i.e., the different contributions interfere with one another. The modulus-square of the sum of all contributions in Figure 6(f) can then be compared to the experimental RCS signal in Figure 6(g). The agreement with the experimental RCS trace is very good, except for three weak peaks marked with red asterisks in Figure 6. These are due to an unidentified contaminant in the sample (possibly 1,2- or 1,3-difluorobenzene), since the same peaks also occur in the supersonic jet spectra.

It is difficult to fit the intensities of the later part of the RCS transient, due to the influence of the J,K-specific collisional dephasing rate constants, which increases with time. These rates are larger for states with small J,K because their energies are smaller (exponential energy gap law).[46,47] While the determination of the J,K-specific rate constants is of great interest, this is extremely difficult because of (1) the enormous number of $J'',K'' \rightarrow J',K'$ microscopic rates involved and (2) the very long fitting times, due to the complexity of the asymmetric-top level structure.

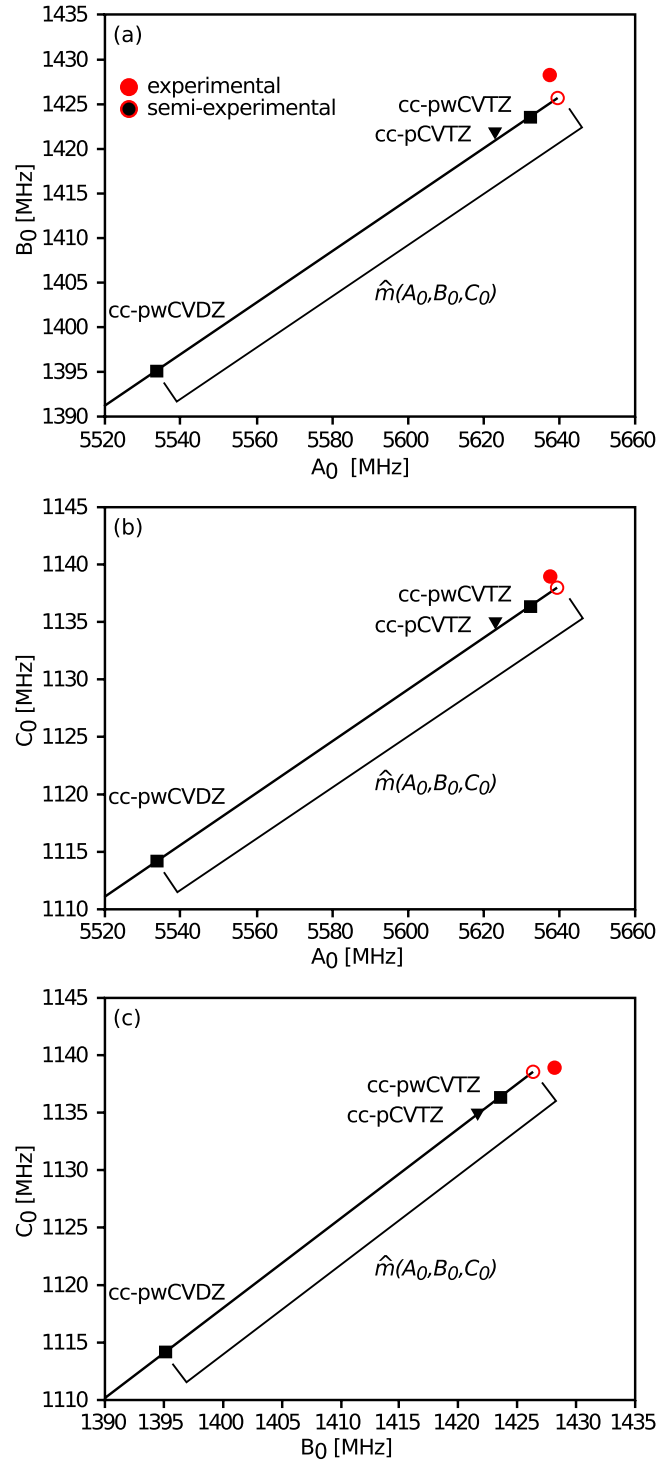

FIG. 7. CCSD(T) *ab initio* calculated and experimental rotational constants A_0, B_0 and C_0, plotted vs. each other. Calculated vibrationally averaged rotational constants from this work indicated by ■, values from Ref. 1 as ▼. The basis-set extrapolation vectors are drawn as black lines, the least-squares extrapolation parameter is $\hat{m} = 1.055$, see the text.

D. Semiexperimental structure determination

Since F has a single stable isotope and since deuterated derivatives were not available in sufficient amounts, it was not possible to solve analytically for the molecular structure based on the rotational constants. However, experimental rotational constants can be combined with those calculated by high-level

TABLE VI. Calculated and semi-experimental equilibrium bond lengths r_e, thermally averaged r_g bond lengths (both in Å), and equilibrium bond angles (in degrees) for *para*-difluorobenzene.

	r_e CCSD(T)				r_e	r_g	r_g
	pwCVDZ	pwCVTZ	pCVTZ[a]	Extrapolation[a,b]	fs-DFWM[c]	fs-DFWM[c,d]	GED[e]
r_e (C_1–C_2)	1.3975	1.3857	1.3868	1.3839	1.3849(4)	1.3891(4)	1.392(2)
r_e (C_2–C_3)	1.4029	1.3925	1.3936	1.3912	1.3917(4)	1.3960(4)	1.392(2)
r_e (C–H)	1.0923	1.0800	1.0804	1.0793	1.0791(5)	1.0822(5)	1.088(5)
r_e (C–F)	1.3500	1.3427	1.3435	1.3431	1.3422(3)	1.3439(3)	1.354(4)
$\angle C_6$–C_1–C_2	121.61	122.09	122.10	122.27	122.11(1)	122.27(1)	123.5(1)
$\angle C_1$–C_2–H	119.20	118.96	118.95	118.87	118.94(1)	119.01(1)	118.25(1)

[a]From Ref. 1.
[b]CCSD(T)/cc-pCVTZ values extrapolated for TZ→ QZ basis set extension by adding the MP2/cc-pwCVQZ–MP2/cc-pCVTZ geometry differences, from Table 11 in Ref. 1.
[c]$\pm 1\sigma$ uncertainties.
[d]fs-DFWM r_e values plus SCF/6-311G(d,p) calculated (r_g–r_e) differences, see the text.
[e]Gas-phase electron diffraction r_g values r_e (C_1–C_2) and r_e (C_2–C_3) were not distinguished in Ref. 9.

ab initio methods to determine a semiexperimental structure by linear basis-set extrapolation, as has been described earlier for symmetric-top molecules for which only one rotational constant is experimentally accessible.[1–3,17,19,20,48] In short, a structural parameter r (bond length, bond angle) is calculated using highly correlated *ab initio* calculations, e.g., the CCSD(T) method using a systematic series of basis sets, e.g. the Dunning correlation-consistent weighted core-valence polarized basis sets series cc-pwCVXZ, where X = 2,3,..., corresponds to the double-zeta, triple-zeta, etc., basis sets. The calculated r structure parameter is expected to asymptotically approach the experimental r value as $X \to \infty$. Assuming linearity r is expressed as $r = r_0 + m(B) * \Delta r$, where the offset r_0 is given by r_{calc} calculated with a smaller basis-set (e.g., cc-pwCVDZ) and the slope Δr is the difference between r_{calc} calculated with a larger (e.g., cc-pwCVTZ) basis set respectively. The parameter $m(B)$ is determined by intersecting the extrapolation vector with the experimental B-value, $B_{sb} + m * \Delta B = B_{exp}$, where B_{sb} is the rotational constant B_{calc} calculated at the small basis and ΔB is the difference between B_{calc} calculated at the large- and small basis respectively.

For asymmetric-rotor molecules for which all three rotational constants are experimentally accessible, the equation for m is over-determined. The standard method to find the "best" value for m (denoted $\hat{m}$) is to employ linear least squares; a more robust estimate of $\hat{m}$ is obtained by employing a weighted version of least squares which accounts for the differences in uncertainty of the experimentally determined rotational constants.[1,48] Geometrically, the least-squares approach corresponds to projecting the set of experimental rotational constants onto the extrapolation vector where one can solve analytically for $\hat{m}$.

Figure 7 shows an orthographic projection of this procedure using the fs-DFWM rotational constants and the corresponding CCSD(T) calculated rotational constants given in Table V. The CCSD(T)/cc-pwCVTZ calculated vibrational ground-state rotational constants A_0, B_0, and C_0 were obtained from the equilibrium rotational constants A_e, B_e, and C_e and the corresponding rotation-vibration coupling constants Δ_A, Δ_B, Δ_C given in Table III. As Figure 7 shows the calculated extrapolation parameter $m = 1.055(27)$ lies not far beyond the CCSD(T)/cc-pwCVTZ value. The basis-set extrapolated semiexperimental bond lengths and angles determined in this way are listed in Table VI.

These semiexperimental bond lengths are smaller than the GED values.[9] This is expected, since GED gives vibrationally averaged structure r_g parameters at the experimental temperature (T = 298 K). To compare the spectroscopic r_e to the GED r_g structure parameters,[9] we calculated the small differences between the r_g and r_e parameters induced by the thermal vibrational averaging, using the second-order perturbation-theory method for calculating r_g structures implemented in the DALTON program.[49,50] Since DALTON employs coupled-pair Hartree-Fock equations for this type of calculation, we calculated the ($r_e - r_g$) values at the Hartree-Fock level, using the 6-311G(d,p) basis set, and combined these with the above-mentioned semiexperimental r_e values, yielding the fs-DFWM semi-experimental r_g values listed in Table VI.

These r_g values differ from those reported by Domenicano *et al.*[9] by −0.003 to −0.004 Å for the C–C bond lengths and by −0.010 Å for the C–F bond length. Also, the C_6–C_1–C_2 ring angle is 122.3° or 1.2° smaller than the GED value. These differences can be partly attributed to the fact that Domenicano *et al.* restricted the C_1–C_2 and C_2–C_3 bond lengths to be equal,[9] whereas we find that C_2–C_3 bond is 0.007 Å longer than the C_1–C_2 bond, in agreement with the prediction of Demaison *et al.*[1] We estimate that the semiexperimental fs-DFWM values are 5–10 times more accurate than the GED values.

IV. CONCLUSIONS

Femtosecond rotational Raman coherence transients detected by four-wave mixing have been measured for *para*-difluorobenzene in a 130 K Ar supersonic jet expansion over time delays up to t = 1400 ps. Analogous measurements were also performed in a room temperature gas-cell at T = 293 K up to t = 2000 ps. The rotational and vibrational cooling of *p*-DFB in the supersonic jet allowed to determine the v = 0 ground-state rotational constants A_0 = 5637.68(19), B_0 = 1428.23(37), and C_0 = 1138.90(48) MHz ($\pm 1\sigma$). While the experimental B_0 and C_0 rotational constants agree with the values predicted by a model approach of Cvitas *et al.*;[10] their estimate of A = 5639.1 MHz differs from our A_0 by 1.4 MHz or 0.1%.

In order to assign RCS features that are associated with different types of rotational coherences, we decomposed the RCS transient into five sub-transients corresponding to coherences with specific rotational quantum number changes ($\Delta J = 0, 1, 2$ combined with $\Delta K = 0, 2$). This decomposition also captures cross-coherence interferences, giving deeper insight than heuristics-based assignments. The sub-transient analysis allowed to characterize a new transient, which we denote *S*-type. It is mainly produced by coherences with $\Delta J = 1/\Delta K = 2$ that occur at delay times $t \sim n/(B + C)$.

Combining the experimental results with CCSD(T)/cc-pwCVXZ (X = 2, 3) calculations also allowed to determine accurate semiexperimental bond lengths and angles. Demaison *et al.*[1] have previously performed CCSD(T) calculations and analyzed the microwave spectroscopic constants of polar fluorobenzenes, and predicted that the two C–C bond lengths of *p*-DFB differ by 0.007 Å. We have obtained the semiexperimental values $r_e(C_1–C_2) = 1.3849(4)$ Å and $r_e(C_2–C_3) = 1.3917(4)$ Å, thereby confirming their predictions.[1] The C–F bond length is r_e(C–F) = 1.3422(3) Å, which differs by only 0.001 Å from that predicted in Ref. 1.

The ability to simulate Raman RCS transients of asymmetric tops will allow to accurately determine the gas-phase structures of strongly asymmetric nonpolar molecules.

ACKNOWLEDGMENTS

Financial support from the Schweiz. Nationalfonds through Grant No. 200020-130376 is gratefully acknowledged.

[1] J. Demaison, H. D. Rudolph, and A. G. Császár, Mol. Phys. **111**, 1539 (2013).
[2] D. S. Kummli, H.-M. Frey, and S. Leutwyler, Chem. Phys. **367**, 36 (2010).
[3] T. S. Den, H. M. Frey, and S. Leutwyler, J. Chem. Phys. **141**, 194303 (2014).
[4] G. Placzek and E. Teller, Z. Phys. **81**, 209 (1933).
[5] A. Weber, "High resolution Raman spectroscopy of gases," in *Handbook of High-Resolution Spectroscopy*, edited by M. Quack and F. Merkt (John Wiley and Sons, Ltd., 2011), pp. 1153–1236.
[6] P. M. Felker and A. H. Zewail, J. Chem. Phys. **86**, 2460 (1987).
[7] P. M. Felker, J. Phys. Chem. **96**, 7844 (1992).
[8] P. M. Felker and A. H. Zewail, "Molecular structures from ultrafast coherence spectroscopy," in *Femtosecond Chemistry*, edited by J. Manz and L. Wöste (VCH, 1995), Vol. 1, Chap. 5.
[9] A. Domenicano, G. Schultz, and I. Hargittai, J. Mol. Struct. **78**, 97 (1982).
[10] T. Cvitas, J. M. Hollas, and H. Kirby, Mol. Phys. **19**, 305 (1970).
[11] T. Cvitas and J. M. Hollas, Mol. Phys. **18**, 793 (1970).
[12] R. Sussmann, R. Neuhauser, and H. Neusser, Can. J. Phys. **72**, 1179 (1994).
[13] C. Riehn, A. Weichert, M. Zimmermann, and B. Brutschy, Chem. Phys. Lett. **299**, 103 (1999).
[14] A. Weichert, C. Riehn, V. V. Matylitsky, W. Jarzeba, and B. Brutschy, J. Mol. Struct. **612**, 325 (2001).
[15] C. Riehn, Chem. Phys. **283**, 297 (2002).
[16] See supplementary material at http://dx.doi.org/10.1063/1.4932602 for Figs. S1, S2 and Table S1.
[17] D. S. Kummli, H. M. Frey, and S. Leutwyler, J. Chem. Phys. **124**, 144307 (2006).
[18] D. S. Kummli, H. M. Frey, and S. Leutwyler, Chimia **60**, 212 (2006).
[19] D. S. Kummli, H. M. Frey, and S. Leutwyler, J. Phys. Chem. A **111**, 11936 (2007).
[20] D. S. Kummli, S. Lobsiger, H. M. Frey, S. Leutwyler, and J. F. Stanton, J. Phys. Chem. A **112**, 9134 (2008).
[21] H.-M. Frey, D. Kummli, S. Lobsiger, and S. Leutwyler, "High-resolution rotational Raman coherence spectroscopy with femtosecond pulses," in *Handbook of High-Resolution Spectroscopy*, edited by M. Quack and F. Merkt (John Wiley & Sons Ltd., Chichester, UK, 2011), pp. 1237–1266.
[22] A. C. Eckbreth, Appl. Phys. Lett. **32**, 421 (1978).
[23] J. F. Stanton, C. L. Lopreore, and J. Gauss, J. Chem. Phys. **108**, 7190 (1998).
[24] J. F. Stanton, J. Gauss, M. E. Harding, and P. G. Szalay, with contributions from A. A. Auer, R. J. Bartlett, U. Benedikt, C. Berger, D. E. Bernholdt, Y. J. Bomble, L. Cheng, O. Christiansen, M. Heckert, O. Heun, C. Huber, T.-C. Jagau, D. Jonsson, J. Jusélius, K. Klein, W. J. Lauderdale, D. A. Matthews, T. Metzroth, D. P. O'Neill, D. R. Price, E. Prochnow, K. Ruud, F. Schiffmann, W. Schwalbach, S. Stopkowicz, A. Tajti, J. Vázquez, F. Wang, J. D. Watts, J. Almlöf, P. R. Taylor, P. R. Taylor, T. Helgaker, H. J. A. Jensen, P. Jørgensen, J. Olsen, A. V. Mitin, and C. van Wüllen, CFOUR, a quantum chemical program package, for the current version, see http://www.cfour.de.
[25] H. M. Frey, P. Beaud, T. Gerber, B. Mischler, P. P. Radi, and A. P. Tzannis, Appl. Phys. B **68**, 735 (1999).
[26] H. M. Frey, P. Beaud, T. Gerber, B. Mischler, P. P. Radi, and A. P. Tzannis, J. Raman Spectrosc. **31**, 71 (2000).
[27] C. Riehn, A. Weichert, and B. Brutschy, J. Phys. Chem. A **105**, 5618 (2001).
[28] H. M. Frey, A. Müller, and S. Leutwyler, J. Raman Spectrosc. **33**, 855 (2002).
[29] P. Hobza, C. Riehn, A. Weichert, and B. Brutschy, Chem. Phys. **283**, 331 (2002).
[30] V. V. Matylitsky, W. Jarzerba, C. Riehn, and B. Brutschy, J. Raman Spectrosc. **33**, 877 (2002).
[31] W. Jarzeba, V. Matylitsky, C. Riehn, and B. Brutschy, Chem. Phys. Lett. **368**, 680 (2003).
[32] C. Riehn, V. Matylitsky, W. Jarzeba, B. Brutschy, P. Tarakeshwar, and K. Kim, J. Am. Chem. Soc. **125**, 16455 (2003).
[33] D. Kummli, H.-M. A. M. Keller, and S. Leutwyler, J. Chem. Phys. **123**, 054308 (2005).
[34] C. Riehn, V. V. Matylitsky, M. F. Gelin, and B. Brutschy, Mol. Phys. **103**, 1615 (2005).
[35] C. Schröter, K. Kosma, and T. Schultz, Science **333**, 1011 (2011).
[36] S. Mukamel, *Principles of Nonlinear Spectroscopy* (Oxford University Press, New York, 1995).
[37] B. Grimberg, V. Lozovoy, M. Dantus, and S. Mukamel, J. Phys. Chem. A **106**, 697 (2002).
[38] E. J. Brown, Q. Zhang, and M. Dantus, J. Chem. Phys. **110**, 5772 (1999).
[39] W. Gordy and R. L. Cook, *Microwave Molecular Spectra* (Wiley, New York, 1984).
[40] C. H. Townes and A. Schawlow, *Microwave Spectroscopy* (Dover Publicatons, Inc., 2012).
[41] D. A. Long, *The Raman Effect* (John Wiley & Sons Ltd., 2002).
[42] P. Joireman, L. C. Connell, S. M. Ohline, and P. M. Felker, J. Chem. Phys. **96**, 4118 (1992).
[43] G. Brügger, H.-M. Frey, P. Steinegger, P. Kowalewski, and S. Leutwyler, J. Phys. Chem. A **115**, 12380 (2011).
[44] J. L. C. Fajin, B. Fernandez, and P. M. Felker, J. Phys. Chem. A **109**, 11602 (2005).
[45] G. Herzberg, *Electronic Spectra and Electronic Structure of Polyatomic Molecules*, Molecular Spectra and Molecular Structure Vol. 3 (Krieger Publishing Company, Malabar, Florida, 1966).
[46] J. C. Polanyi and K. B. Woodall, J. Chem. Phys. **56**, 1563 (1971).
[47] I. Procaccia and R. Levine, J. Chem. Phys. **63**, 4261 (1975).
[48] J. Demaison, Mol. Phys. **105**, 3109 (2007).
[49] K. Aidas, C. Angeli, K. L. Bak, V. Bakken, R. Bast, L. Boman, O. Christiansen, R. Cimiraglia, S. Coriani, P. Dahle, E. K. Dalskov, U. Ekström, T. Enevoldsen, J. J. Eriksen, P. Ettenhuber, B. Fernández, L. Ferrighi, H. Fliegl, L. Frediani, K. Hald, A. Halkier, C. Hättig, H. Heiberg, T. Helgaker, A. C. Hennum, H. Hettema, E. Hjertenæs, S. Høst, I.-M. Høyvik, M. F. Iozzi, B. Jansík, H. A. Jensen, D. Jonsson, P. Jørgensen, J. Kauczor, S. Kirpekar, T. Kjærgaard, W. Klopper, S. Knecht, R. Kobayashi, H. Koch, J. Kongsted, A. Krapp, K. Kristensen, A. Ligabue, O. B. Lutnæs, J. I. Melo, K. V. Mikkelsen, R. H. Myhre, C. Neiss, C. B. Nielsen, P. Norman, J. Olsen, J. M. H. Olsen, A. Osted, M. J. Packer, F. Pawlowski, T. B. Pedersen, P. F. Provasi, S. Reine, Z. Rinkevicius, T. A. Ruden, K. Ruud, V. V. Rybkin, P. Sałek, C. C. M. Samson, de A. S. Merás, T. Saue, S. P. A. Sauer, B. Schimmelpfennig, K. Sneskov, A. H. Steindal, K. O. Sylvester-Hvid, P. R. Taylor, A. M. Teale, E. I. Tellgren, D. P. Tew, A. J. Thorvaldsen, L. Thøgersen, O. Vahtras, M. A. Watson, D. J. D. Wilson, M. Ziolkowski, and H. Ågren, Wiley Interdiscip. Rev.: Comput. Mol. Sci. **4**, 269 (2014).
[50] P.-O. Astrand, K. Ruud, and P. R. Taylor, J. Chem. Phys. **112**, 2655 (2000).